

Phys. Rev. Lett. 97 (2006)

Real-Time Ab Initio Simulations of Excited Carrier Dynamics in Carbon Nanotubes

Yoshiyuki Miyamoto,¹ Angel Rubio,² and David Tománek³

¹Fundamental and Environmental Research Laboratories,
NEC Corp., 34 Miyukigaoka, Tsukuba, 305-8501, Japan

²Dpto. Física de Materiales, UPV/EHU,
Centro Mixto CSIC-UPV/EHU, DIPC, 20018 San Sebastián,
Spain, and European Theoretical Spectroscopy Facility (ETSF)

³Department of Physics and Astronomy,
Michigan State University, East Lansing, Michigan 48824-2320

(Dated: April 15, 2024)

Abstract

Combining time-dependent density functional calculations for electrons with molecular dynamics simulations for ions, we investigate the dynamics of excited carriers in a (3,3) carbon nanotube at different temperatures. Following an $h\nu = 6.8$ eV photoexcitation, the carrier decay is initially dominated by efficient electron-electron scattering. At room temperature, the excitation gap is reduced to nearly half its initial value after 230 fs, where coupling to phonons starts dominating the decay. We show that the onset point and damping rate in the phonon regime change with initial ion velocities, a manifestation of temperature dependent electron-phonon coupling.

PACS numbers: 81.07.De, 82.53.Mj, 73.22.-f, 73.63.Fg

Understanding the microscopic decay mechanism of electronic excitations is a challenging problem in nanotechnology. The fundamental hurdle is the requirement of unprecedented computational resources to treat the time evolution of electronic and ionic degrees of freedom in real time, from first principles, for physically relevant time periods. Carbon nanotubes are the ideal system to study these effects due to their well-defined structure, intriguing electronic properties [1], and a high potential for application in future electronic devices [2]. Additional interest has recently been triggered by observing optical emission induced by an electric current [3], radio-wave emission from aligned nanotubes working as an antenna [4], and potential application of nanotubes in a mode-locked laser [5]. Whether studying the nature of excitonic effects affecting photoabsorption [6], or attempting to identify the maximum switching frequency of future field-effect transistors or lasers, the key to progress is to understand the lifetime of excited carriers in carbon nanotubes.

Time-resolved femtosecond pump-probe spectroscopy, applied to nanotube samples, has identified two regimes in the decay of carrier excitations [7]. An ultra-fast decay channel has been associated with electron-electron scattering, which causes an internal thermalization of the electronic system within 200 fs. A slower decay channel has been associated with the excitation of ionic degrees of freedom at later times. Extracting information about carrier decay in specific, isolated nanotubes from those pump-probe data is not straight-forward, since samples contain a mixture of metallic and semiconducting nanotubes with different diameters and chiralities, all of which interact with the substrate.

Here we present the first *ab initio* real-time calculation of the decay mechanism of electronic excitations in narrow carbon nanotubes, which exhibit strong electron-phonon coupling [8, 9]. In our approach, we treat the time dependence of the electronic degrees of freedom using time-dependent density functional theory (TDDFT) [10]. Unlike in previous parameterized TDDFT calculations [11], we determine concurrently the ionic motion in the evolving charge density distribution by direct integration using molecular dynamics (MD) simulations within the force field given by the density functional theory (DFT). Our results provide not only an unbiased interpretation of available experimental data, but also identify the time scales associated with the dominant carrier decay channels and their temperature dependence. Our conclusion that the excitation gap is reduced by electron-electron scattering first, followed by electron-phonon interaction, is general and not restricted to narrow carbon nanotubes.

Alternatively, selected aspects of excited carrier dynamics could be described by summing up all diagrams corresponding to the electron-electron and electron-phonon many-body interactions. Under steady-state conditions, where the Fermi golden rule and Boltzmann transport picture apply [12], electron-phonon coupling can be determined by integrating the scattering matrix elements for transitions involving particular phonon modes. The corresponding scattering time constant, including its temperature dependence, could then be determined using the inverse momentum-space integrals of these matrix elements [13]. This steady-state approach, however, is not applicable in the sub-picosecond regime of interest here, since electron-electron scattering processes have been averaged out. Dynamics of electronic decay channels only, ignoring coupling to phonons, could also be inferred from the imaginary part of the electron self-energy, determined using the GW approximation [14].

Unlike these approaches, our calculations offer an unbiased insight into the short-time dynamics of electronic excitations, since electron and phonon scattering are treated on the same footing in real time within TDDFT-MD, using the FPSEID (First Principles Simulation tool for Electron Ion Dynamics) code [15]. Since the systems of interest are well above zero temperature, the ionic motion is described classically, with the forces acting on the ions given by the density functional theory in the local density approximation (LDA) [16]. The electron-ion interaction is described using norm-conserving soft pseudopotentials [17], and the valence wave functions are expanded in a plane wave basis with a kinetic energy cutoff of 40 Ry.

To allow for a realistic representation of phonons in isolated (3,3) nanotubes, we arrange 96-atom supercells, which extend over eight primitive unit cells of the tube, in a hexagonal geometry with an inter-wall separation of 5 Å. We find that Γ point sampling of the small Brillouin zone is sufficient to describe the electron-electron and electron-phonon coupling well. To describe the dynamics at a given temperature, we randomize the initial ion velocities according to the Maxwell-Boltzmann distribution for that thermodynamical ensemble. The excited-state dynamics then proceeds in three steps. First, we simulate the initial optical excitation by promoting a valence electron to an unoccupied Kohn-Sham (KS) state. Next, by fixing this electronic configuration, we use constrained DFT to determine the electronic structure in that excited state. Finally, we continue a full, unconstrained TDDFT-MD simulation starting with these initial ion velocities and charge distribution.

Figure 1 depicts the electronic structure and photoabsorption spectrum in the narrow

(3;3) carbon nanotube [18]. The electronic band structure of the primitive unit cell, shown in Fig. 1 (a), agrees with published data [19, 20] also in displaying the curvature effect, which modifies the Fermi momentum from the zone folding value at $2=3(\pi/a)$. The photoabsorption spectrum in Fig. 1 (b) displays the response to light with the E-field polarized along the tube axis. Since depolarization effects normal to the tube are not important due to the small cross-section [20], we used Fermi's golden rule directly to calculate the optical dipole matrix elements between occupied and empty KS eigenstates [21].

We found two relevant photoabsorption processes, labelled 'A' and 'B' in Fig. 1. The absorption spectrum is dominated by a peak labeled 'A' [19], which stems from many independent electron-hole transitions in a narrow energy range. A complex competition between the electronic decay channels, each with a different time constant, and phonon decay channels makes a clear distinction between electronic and phonon contributions problematic and will not be attempted here. In the following, we rather focus on the transition labelled 'B' in Fig. 1, which, in spite of its smaller oscillator strength, is better defined due to the absence of nearby transitions with a large oscillator strength and allows a clear distinction between electronic and ionic decay channels. Our findings in terms of dominant decay channels, we believe, are of general nature, applicable to other photoabsorption processes in related systems.

The time evolution of the electronic spectrum following a 'B' excitation at $t = 0$ is shown in Fig. 2. The time evolution of the KS eigenvalues indicates a rapid reduction of the electron-hole excitation gap [22] to less than half its initial value of 6.8 eV within 500 fs from the photoexcitation. The individual electron (hole) eigenvalues show an initial tendency to reach the bottom (top) of the conduction (valence) band very rapidly, manifesting the efficient non-radiative decay of the optical excitation towards the lowest lying electronic excitation. Under room temperature conditions, depicted in Fig. 2 and achieved by initially thermalizing the ionic motion at $T = 300$ K, we find a noticeable reduction of the decay rate to 230 fs after the photoexcitation. Subsequent decay may involve less efficient radiative transitions [6] or energy transfer to phonons.

We believe that the predicted reduction of the electron-hole energy gap could in principle be observed in time-resolved experiments. Light emission as a result of electron-hole recombination could generally be expected, since the computed optical matrix elements between the excited electron and hole states fluctuate for a long time around a finite value. Even

though non-radiative decay of the excitation towards the lowest excitonic state is typically faster than radiative decay, emission could possibly be resonantly enhanced by the probe laser.

To gain additional insight into the electronic decay, including possible radiative transitions, we investigated the time evolution of the matrix containing electron-hole dipole matrix elements. Immediately after the photoexcitation, the only non-vanishing matrix elements involve a field along the tube axis, same as in the initial photo-absorption. Later on, as phonons weakened the dipole selection rules, we observed matrix elements involving a field normal to the tube axis to increase, and eventually to reach similar values as those involving a field along the tube axis. As the electron-hole dipole matrix elements become isotropic in time, also the radiative decay should not show any preferential polarization.

In spite of substantial changes in its electronic structure, the (3;3) nanotube retains its cylindrical shape throughout the simulation. Close inspection of the vibrational spectra indicates enhancement of particular phonon modes following the photoexcitation, in particular at $\omega = 556 \text{ cm}^{-1}$, close to the $\omega_{\text{RBM}} = 536 \text{ cm}^{-1}$ value reported for the radial breathing mode (RBM) of the (3;3) carbon nanotube [9]. Our conclusion that the RBM may be excited by photoabsorption is also supported by recent femtosecond pump-probe experiments, which report exciting coherent phonons, including the RBM, in semiconducting single wall carbon nanotubes using resonant sub-10 fs pulses in the visible range [23].

The time-dependence of the photoexcitation gap, discussed in conjunction with Fig. 2, tells little about the nature and temperature dependence of the processes controlling the hot carrier decay. To obtain this information, we investigated the photo-decay in nanotubes with initial ionic temperatures of $T = 77 \text{ K}$, 150 K , and 300 K . Witnessing to the numerical long-time stability of our TDDFT-MD simulations, we find the total energy to be conserved with a maximum deviation of about 10^{-3} eV/atom over the 0.5 ps long simulations. Figure 3 depicts the key result, namely the time dependence of the potential energy of the nanotube under different initial conditions.

Due to the finite size of our unit cell, the potential energy fluctuates in time, with larger fluctuations occurring at higher temperatures. Since ensemble averaging over many runs would necessitate unreasonably large computer resources, we invoked ergodicity and time averaged our potential energy profiles over 50 fs long time periods. Our results, displayed by the dotted lines in Fig. 3, indicate that independent of the initial temperature, the potential

energy decreases in time. After reaching a cross-over point, an initially gradual decrease becomes steeper. We find the decay rate to be nearly linear in both regimes, as shown by the dashed lines in Fig. 3. Whereas the decay rate in the early regime is rather independent of the initial temperature, its length decreases from 360 fs at 77 K to 230 fs at 300 K. Also, in the regime beyond the cross-over point, the decay rate decreases with increasing temperature, suggesting a slower energy flow from the electronic system to the ionic lattice. This is a clear indication of a temperature-dependent electron-phonon coupling.

In contrast to the time dependence of the potential energy discussed above, the electron-hole energy gap, shown in Fig. 2, first shows a rapid, then a more gradual decrease. The cross-over points between the two decay regimes at 300 K, based on the electronic spectra in Fig. 2 and the potential energy in Fig. 3, nearly coincide at $t = 230$ fs, suggesting the same underlying mechanism. Our finding that the initial decay is fast in Fig. 2, yet slow and temperature independent in Fig. 3, suggests that early decay regime is dominated by relaxations within the electronic system only. The opposite behavior is observed in the second regime, suggesting involvement of phonons. In view of the stronger electron-phonon coupling in the narrow (3;3) nanotube, our estimated cross-over point between the regimes should still remain valid as a lower limit for wider nanotubes. In view of uncertainties associated with samples containing mixtures of nanotubes, the value $t = 200$ fs, observed [7] in single-wall nanotubes with diameters close to 1.2 nm, lies very close to our prediction.

Even though the time evolution of the charge density, underlying the density functional force field on the ions, is based on Ehrenfest dynamics [24], our calculated forces do reflect the electron and ion dynamics at particular temperatures without relying on the adiabatic potential energy surface for a particular excited state. Deviations from Ehrenfest dynamics only occur, when the system cannot be associated with the adiabatic potential energy surface of an individual excited state. This would give rise to non-vanishing off-diagonal matrix elements of the time-dependent Kohn-Sham matrix, evaluated in the basis of the corresponding time-dependent eigenstates. We have indeed observed such non-vanishing off-diagonal matrix elements, albeit very small in magnitude, and only during short time periods in our simulation [25]. As another point worth mentioning, the electron-hole attraction in excitonic states, which is not reproduced by the DFT, is known not to change the total charge density much and thus not to affect the electron and ion dynamics. Thus, in stark contrast to the strong influence of ions on the excited carriers, which we consider explicitly, we find

the influence of electronic excitations on the ion dynamics to be negligible. All the above arguments, along with the high degree of total energy conservation in our system discussed earlier, justify our use of Ehrenfest dynamics.

In conclusion, our large-scale *ab initio* simulations of photophysical processes in carbon nanotubes suggest that the decay of photoexcited carriers occurs on a sub-picosecond time scale. An initial rapid nonradiative electronic decay is followed by a temperature-dependent, slower decay involving phonons. The duration of the electronic decay regime and the decay rate in the phonon-dominated regime decrease with increasing temperature, suggesting temperature-dependent electron-phonon coupling.

YM acknowledges fruitful discussions with Dr. B.D. Yu and major use of the Earth Simulator Supercomputer. AR was supported by the EC projects NANOQUANTA (NMP4-CT-2004-500198), SANES (NMP4-CT-2006-017310), Spanish MCyT, and the Humboldt Foundation. DT was supported by NSF NIRT grants DMR-0103587, ECS-0506309, NSF NSEC grant EEC-425826, and the Humboldt Foundation.

-
- [1] M. S. Dresselhaus, G. Dresselhaus, and Ph. Avouris (Eds.): Carbon nanotubes: synthesis, structure, properties, and applications, Springer-Verlag Berlin 2001.
 - [2] S. Heinze, J. Terso, R. Martel, V. Derycke, J. Appenzeller, and Ph. Avouris, Phys. Rev. Lett. 89, 106801 (2002); F. Nihey, H. Hongo, M. Yudasaka, and S. Iijima, Jpn. J. Appl. Phys. 41, L1049 (2002).
 - [3] J. Amisevich, et al., Science 300, 783 (2003).
 - [4] Y. Wang et al., Appl. Phys. Lett. 85, 2607 (2004).
 - [5] S.Y. Set et al., Proc. of Optical Fiber Communication Conference 2003, March 23–28 (2003).
 - [6] F. Wang, G. Dukovic, L.E. Brus and T.F. Heinz, Science 308, 838 (2005), and references therein.
 - [7] T. Hertel and G. Mios, Phys. Rev. Lett. 84, 5002 (2000); A. Hagen, G. Mios, V. Talabev, and T. Hertel, Appl. Phys. A 78, 1137 (2004); L. Huang, H.N. Pedrosa, and T.D. Krauss, Phys. Rev. Lett. 93, 017403 (2004); Y.-Z. Ma et al., J. Chem. Phys. 120, 3368 (2004).
 - [8] L.X. Benedict, V.H. Crespi, S.G. Louie, and M.L. Cohen, Phys. Rev. B 52, 14935 (1995); M. Ichida, et al., Physica B 323, 237 (2002).

- [9] K.P. Bohnen, R. Heid, H.J. Liu, and C.T. Chan, Phys. Rev. Lett. 93, 245501 (2004). D. Connetable, G.M. Rignanes, J.C. Charlier, X. Blase, *ibid* 94, 015503 (2005).
- [10] E. Runge and E.K.U. Gross, Phys. Rev. Lett. 52, 997 (1984).
- [11] T.A. Niehaus, D. Heringer, B. Torralva and Th. Frauenheim, Europ. Phys. J. D 35, 467 (2005).
- [12] V. Perebeinos, J. Terso, and P. Avouris, Phys. Rev. Lett. 94, 86802 (2005).
- [13] J. Jiang et al., Phys. Rev. B 71, 45417 (2005).
- [14] C.D. Spataru, M.A. Cazalilla, A. Rubio, L.X. Benedict, P.M. Echenique, and S.G. Louie, Phys. Rev. Lett. 87, 246405 (2001).
- [15] O. Sugino and Y. Miyamoto, Phys. Rev. B 59, 2579 (1999); *ibid*, Phys. Rev. B 66 89901 (E) (2002).
- [16] J.P. Perdew, A. Zunger, Phys. Rev. B 23, 5048 (1981); D.M. Ceperley, B.J. Alder, Phys. Rev. Lett. 45, 566 (1980).
- [17] N. Troullier, J.L. Martins, Phys. Rev. B 43, 1993 (1991); L. Kleinman and D.M. Bylander, Phys. Rev. Lett. 48, 1425 (1982).
- [18] Even though free-standing (3;3) nanotubes have not been reported, calculations indicate that they are stable. Optical spectroscopy also confirms that such narrow nanotubes may form inside pores of a zeolite [19].
- [19] Z.M. Li, et al., Phys. Rev. Lett. 87, 127401 (2001).
- [20] A.G. Marinopoulos, L. Reining, A. Rubio, and N. Vast, Phys. Rev. Lett. 91, 046402 (2003).
- [21] The photoabsorption spectrum was obtained by sampling the Brillouin zone with 16 k-points. For quantitative agreement with experiment, the spectrum in Fig. 1(b) should include self-energy and excitonic effects which are beyond the scope of this work.
- [22] Taking total energy differences based on constrained LDA calculations, we found the electron-hole excitation gap corresponding to transition $\Gamma \rightarrow \Gamma$ to lie at 6.89 eV, close to the Koopman's Theorem value of 6.8 eV.
- [23] C. Manzoni et al., Phys. Rev. Lett. 94, 207401 (2005); A. Gambetta et al., Nature Phys. 2, 515 (2006).
- [24] P. Ehrenfest, Z. Phys. 45, 455 (1927).
- [25] See EPAPS document No. XXXX for the time dependence of the off-diagonal matrix elements of the Kohn-Sham matrix.

Figures

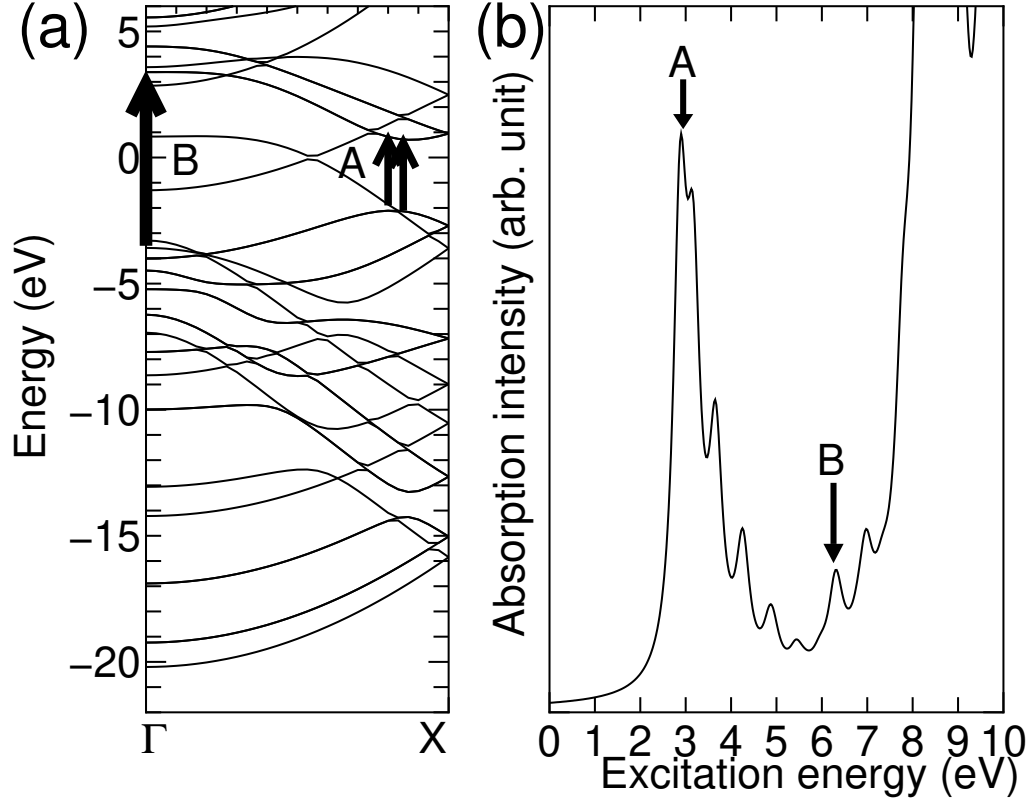


FIG .1: (a) LDA band structure and (b) optical absorption spectrum of an isolated (3;3) nanotube for a dipole eld along the tube axis. Two dipole-allowed transitions are labelled 'A' and 'B'. The Fermi level lies at 0 eV .The absorption spectrum (b) has been convoluted with a 0.3 eV wide Lorentzian .

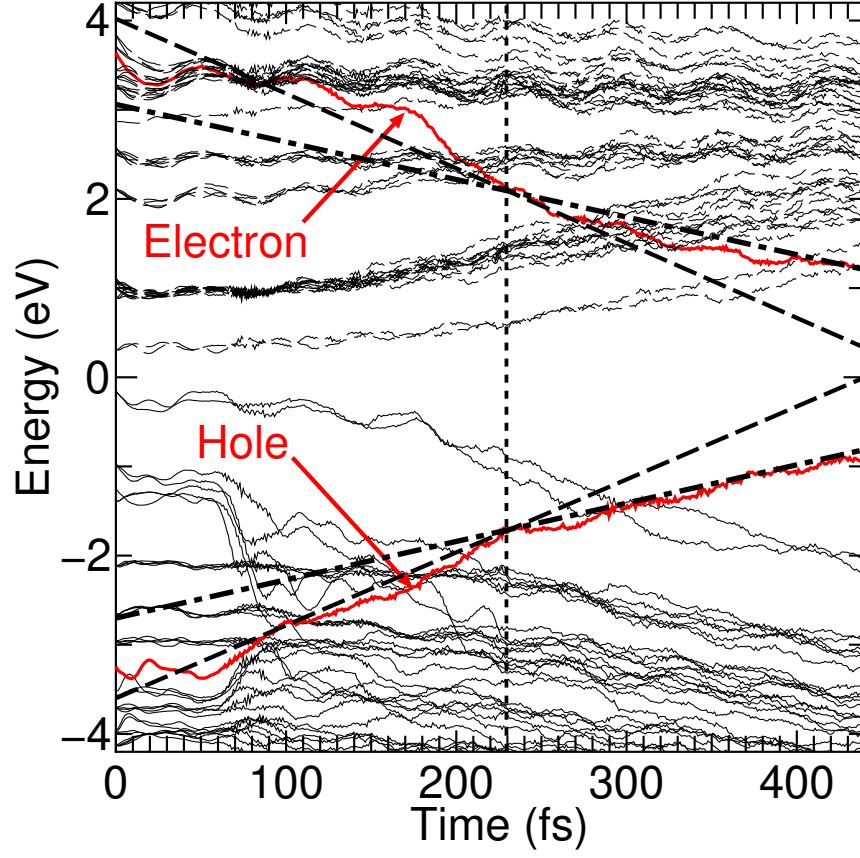


FIG. 2: (Color online) Dynamics of hot-carrier decay following the excitation labelled 'B' in Fig. 1, after the ions have been thermalized at $T = 300$ K. Valence bands are shown by solid lines and conduction bands by dotted lines. The excited electron and hole states are shown by heavy solid lines. Dashed lines are guides to the eye.

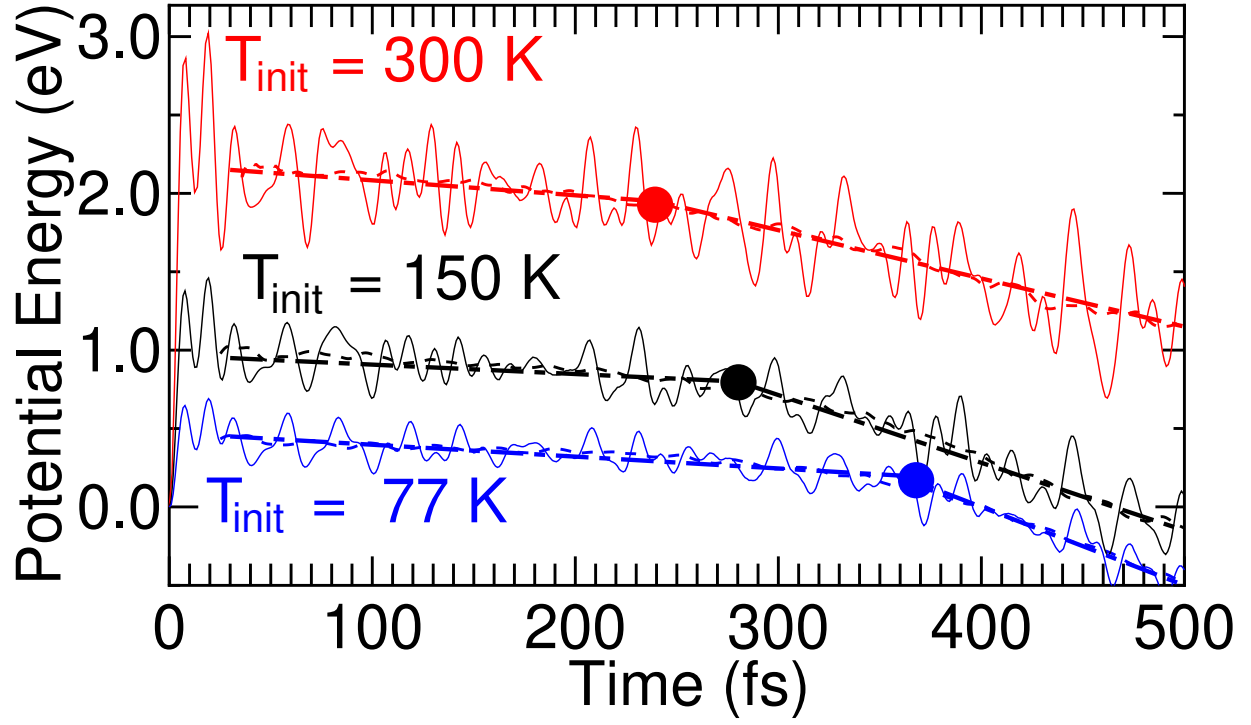


FIG. 3: (Color online) Time dependence of the ionic potential energy after the photoexcitation at $t = 0$. The different solid lines describe systems with an initial Maxwell-Boltzmann velocity distribution corresponding to $T = 77$ K, 150 K, and 300 K. The light dotted lines represent time-averaged values. The dashed lines, showing linear fits to the data, are guides to the eye to distinguish the two time regimes.